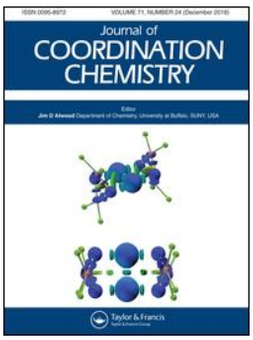

Taylor & Francis
Taylor & Francis Group

Journal of Coordination Chemistry

ISSN: (Print) (Online) Journal homepage: https://www.tandfonline.com/loi/gcoo20

Subtle variation of stereo-electronic effects in rhodium(I) carbonyl Schiff base complexes and their iodomethane oxidative addition kinetics

Pennie P. Mokolokolo , Alice Brink , Andreas Roodt & Marietjie Schutte-Smith

To cite this article: Pennie P. Mokolokolo , Alice Brink , Andreas Roodt & Marietjie Schutte-Smith (2020): Subtle variation of stereo-electronic effects in rhodium(I) carbonyl Schiff base complexes and their iodomethane oxidative addition kinetics, Journal of Coordination Chemistry, DOI: 10.1080/00958972.2020.1809657

To link to this article: https://doi.org/10.1080/00958972.2020.1809657

JOURNAL OF COORDINATION CHEMISTRY
https://doi.org/10.1080/00958972.2020.1809657

Taylor & Francis
Taylor & Francis Group

Subtle variation of stereo-electronic effects in rhodium(I) carbonyl Schiff base complexes and their iodomethane oxidative addition kinetics

Pennie P. Mokolokolo, Alice Brink, Andreas Roodt and Marietjie Schutte-Smith

Department of Chemistry, University of the Free State, Bloemfontein, South Africa

ABSTRACT

Rhodium(I) carbonyl complexes of the form [Rh^{I}(*N,O*-ScBa)(CO)(PR_3)] (R = Ph or Cy), with *N,O*-ScBaH a mono anionic bidentate Schiff base ligand, 2-(cyclopentyliminomethyl)-5-methylphenol (5-Me-Sal-CyPH), and bearing different phosphine ligands on Rh(I), are reported. *N,O*-ScBaH was also varied to be 2-(cyclohexyliminomethyl)phenol (Sal-CyH) and 2-(isopropyliminomethyl)-5-methylphenol (5-Me-Sal-IPropH) to investigate the effects of different substituent groups on the periphery of the Schiff bases on metal center reactivity. The structural characterization of two sample complexes is described and an extensive spectroscopic kinetic-mechanistic study utilizing UV/vis, infrared and ^{31}P NMR spectroscopy of the iodomethane oxidative addition is presented. Iodomethane oxidative addition led exclusively to Rh^{III}-alkyl complexes as final products, while an associative activation is inferred from the large negative $\Delta S^{\neq}$ value. The relative reactivity of the [Rh^{I}(*N,O*-ScBa)(CO)(PR_3)] complexes when stepwise varying PR_3 (PPh_3, PPh_2Cy, $PPhCy_2$ and PCy_3) as tertiary phosphine ligands follow a surprising similar reactivity relationship as observed for a range of isostructural [Rh^{I}(*X,O*-Bid)(CO)(PR_3)] complexes, with X = O, N or S in corresponding oxinate, acetylacetonate and thioureate mono anionic *X,O*-Bid ligands. This suggests systematic and responsive dynamic behavior of the PR_3 ligands, *independent* of the bidentate chelate at the Rh(I) metal center. A variation of more than two orders-of-magnitude in reactivity was observed.

ARTICLE HISTORY
Received 28 May 2020
Accepted 30 July 2020

KEYWORDS
Structure/reactivity relationships; Schiff base ligands; rhodium phosphine; kinetics

CONTACT Alice Brink brinka@ufs.ac.za; Andreas Roodt roodta@ufs.ac.za Department of Chemistry, University of the Free State, PO Box 339, Bloemfontein 9300, South Africa
Dedicated to the memory of Professor Enbo Wang.

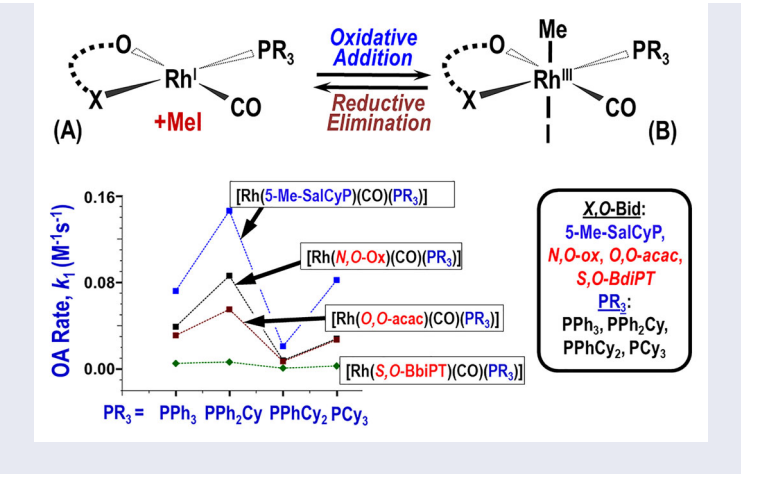

1. Introduction

Schiff bases may be considered a sub-class of imines, thus either secondary aldimines or secondary ketimines, depending on their structure. It is often synonymous with azomethine when referring more specifically to secondary aldimines (i.e. R-CH = NR' where R' ≠ H). Named after Hugo Schiff, and having been around for more than 155 years [1–3], they are still relevant in (modern) coordination chemistry [4,5], showing potential for application in carbon dioxide utilization [6]. Some recent papers and reviews (not exhaustive) detailing aspects of these are available [7–10].

Oxidative addition reactions on metal complexes represent key steps in many catalytic processes, including the carbonylation of alcohols, hydroformylation of alkenes and cross-coupling reactions [11,12]. A classic example is the rhodium/iridium-iodide supported carbonylation of methanol to produce acetic acid, i.e. the so-called Monsanto and Cativa processes [13,14]. Oxidative addition is suggested as the rate-determining step in the catalytic cycles of some of these processes, and therefore any influence on this step can determine the course of the complete catalytic cycle. Due to the vital role of this reaction, a significant amount of research has focused on oxidative addition reactions to understand its kinetic properties and responses to external and internal ligand influences [15,16]. In the Monsanto process the metal carbonyl species is $[Rh^{I}(I)_2(CO)_2]^-$, which is relatively unstable.

On the other hand, rhodium carbonyl species containing tertiary phosphine ligands and/or bidentate ligands are generally more stable, with interesting recent metallophilic/non-covalent interactions described in selected Rh(I) dicarbonyl complexes [17]. By tuning the stereo-electronic properties of both the bidentate and the tertiary phosphine ligands, the carbonylation process may be directed towards different outcomes. For example, other products might arise if hydrogenation precedes the reductive elimination. Numerous studies have been undertaken to improve the catalytic activity of the rhodium-based complex by introducing ligands with different electronic and steric properties, which also include variation of the bite angle of the bidentate ligand [15]. Increasing the electron density on the rhodium center can activate it towards

oxidative addition since the metal is a nucleophile in these reactions, although the steric effects associated with any changes are equally important and may counter-act the advantages of a more nucleophilic metal.

Complexes of the type [Rh(*L,L'*-Bid)(CO)(PR_3)], where *L,L'*-Bid = monoanionic bidentate ligands and PR_3 are tertiary phosphine ligands, have thus been investigated extensively as potential catalyst precursors [18–26]. In the case where bidentate ligands contain a sulfur donor, for example thioacetylacetone [20], the iodomethane oxidative addition primarily led to Rh^{III}-acyl complexes [27–29]. This was also confirmed for other *S,O*-Bid ligand systems (notably thiourea based (*S,O*-BidH = *N*-benzoyl-*N'*,*N'*-diphenylthiourea) [23]. In both these ligand systems, however, the overall net reaction rate was slowed significantly due to the associated steric effect introduced by the bidentate ligand.

For the present study coordinated Schiff base bidentate ligand systems and their effect on the oxidative addition reaction are considered. We opted to investigate these *N,O*-donor ligands, since they allow *six-membered metallacycle* non-labile bidentate entities, and limited detailed kinetic data are available for Rh-Schiff base ligand systems [10,30]. The structural flexibility of these ligands offers prospects of controlling (i) the denticity of the final ligands, (ii) the nature of donor atoms, (iii) the number of chelating moieties and (iv) the ease of manipulating the (outer) periphery of the ligand. They therefore afford an opportunity to manipulate the activity, reactivity and selectivity of catalyst models through ligand optimization strategies [31,32]. For the current study, varying electronic and steric parameters as informed by the cyclopentyl, cyclohexyl, and isopropyl substituents attached to the imine nitrogen introduced on the targeted Schiff base ligands to investigate how these entities will affect the rate of oxidative addition. This paper also evaluates the effect on the rate of oxidative addition when systematically interchanging the phenyl groups for the cyclohexyl groups on the tertiary phosphine ligand in conjunction with varying the Schiff bases. Since much current 'mechanistic research' involves purely the analysis of reactants and products, while the time-resolved details are much less studied, we here emphasize yet again the importance of detailed structure-*reactivity* studies in fundamental reactions to catalytic processes to ensure a more elaborate and complete analysis.

2. Results and discussion

2.1. Synthesis

A series of bidentate Schiff base ligands (*N,O*-ScBaH), 2-(cyclopentyliminomethyl)-5-methylphenol (5-Me-Sal-CyPH) (**I**), 2-(cyclohexyliminomethyl)phenol (Sal-CyH) (**II**), and 2-(isopropyliminomethyl)-5-methylphenol (5-Me-Sal-IpropH) (**III**) were synthesized using the procedure previously reported [31,33]. The steric and electronic subtleties in these Schiff base ligand systems were pursued through the introduction of methyl, cyclopentyl, isopropyl and cyclohexyl substituents on the ligand periphery. The rhodium(I) complexes, [Rh(*N,O*-ScBa)(CO)(PR_3)] (PR_3 = monophosphine ligands), were synthesized as reported previously by heating a DMF solution of $RhCl_3{\cdot}xH_2O$ (Scheme 1), followed by addition of the respective Schiff base ligand and precipitation of the [Rh(*N,O*-ScBa)$(CO)_2$] precursors (**1**, **2**, **3**). Complexes **1a**, **2a** and **3a** were obtained by

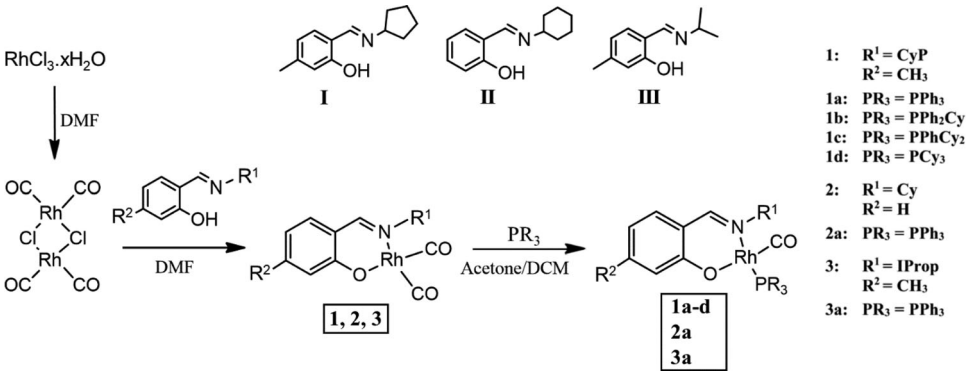

Scheme 1. General synthesis of Rh(I)-carbonyl monophosphine Schiff base complexes, [Rh(*N,O*-ScBa)(CO)(PR_3)] (**1a-d**; **2a**, **3a**), via the dicarbonyl complexes (**1**-**3**) containing *N,O*-ScBaH: 2-(cyclopentyliminomethyl)-5-methylphenol (**I**), 2-(cyclohexyliminomethyl)phenol (**II**) and 2-(isopropyliminomethyl)-5-methylphenol (**III**).

reacting the different Schiff base dicarbonyl complexes with the corresponding tertiary phosphine ligand in acetone/DCM solution.

Similarly, in order to study the effect of the different substituted tertiary phosphine ligands (PR_3) on the rate of the oxidative addition reaction, [Rh(5-Me-Sal-CyP)$(CO)_2$] (**1**) was reacted with the range of monophosphine ligands to yield the corresponding [Rh(*N,O*-ScBa)(CO)(PR_3)] complexes (Scheme 1; **1a**-**d**).

2.2. IR and ^{31}P-NMR spectroscopy

All the rhodium(I) monophosphine complexes were characterized by IR and ^{31}P-NMR spectroscopy and the corresponding data are presented in Table 1. The Rh-CO stretching frequency serves as an excellent measure of the electron density on the rhodium and a way of identifying the reactants and products present. Complexes **1**(**a**-**d**), **2a** and **3a** showed a characteristic single carbonyl absorbance peak (1937-1957 cm^{-1}), indicative of the exclusive formation of only one isomer, with the phosphine ligand *trans* to the nitrogen of the chelating bidentate ligand as indicated by X-ray crystallographic studies. Previous studies have indicated that the *trans* influence for oxygen, nitrogen and sulphur follows the reverse electronegativity range, i.e. S > N > O [20,34,35]. This general trend can however have different variations as a variable order of substitution has been noted for electron-withdrawing phosphite ligands that are sterically less demanding [36–38]. The formation of only one isomer product is further supported by the ^{31}P-NMR, as only one doublet is observed between 53 and 41 ppm (Supporting Information). The first-order rhodium-phosphorus coupling ($^1J_{Rh\text{-}P}$) thus obtained, together with the Rh-CO IR stretching frequency values of **1a**, **2a** and **3a**, allow concluding that the peripheral substituents on the Schiff base ligand backbone do not have a significant effect on the electron density on the rhodium center.

The infrared data in Table 1 show a decrease in the observed Rh-CO stretching frequency as one moves from PPh_3 to PCy_3 (**1a**-**d**). This behavior is in agreement with the increase in pK_a values of the monophosphine ligands (3.28, 5.87, 8.46 and 11.3 for

Table 1. Summary of spectroscopic data for 1(a-d), 2a and 3a.

	PR_3	1a	1b	1c	1d	2a	3a
IR: ν_{CO}	**(cm^{-1})**	1955	1945	1943	1937	1957	1955
^{31}P NMR: δ	**(ppm)**	41.5	49.5	53.8	50.2	41.6	41.5
$^{1}J_{Rh\text{-}P}$	**(Hz)**	158	156	156	151	157	159

PPh_3, PPh_2Cy, $PPhCy_2$ and PCy_3, respectively) [39] since the higher the pK_a value, the more nucleophilic the phosphorus becomes. This in turn results in an increase in electron density on rhodium upon coordination of the phosphine ligands, and translates to an increase in π-backbonding, leading to a lower wavenumber in IR absorption, as well as corresponding changes in the chemical shift of the ^{13}P signals.

2.3. X-ray crystallography

Perspective diagrams of the crystallographically determined geometries for the monophosphine complexes **1a** and **2a** showing the atom numbering scheme used are given in Figure 1. Single crystals were obtained by slow evaporation of an acetone/dichloromethane solution. Despite our best efforts, no crystals suitable for X-ray diffraction analysis could be obtained for **3a**, nor for any of the alkyl products **4a**-**d**, **4e** or **4f**. The basic data collection parameters are provided while important bond distances and angles are listed in Table 2.

The neutral rhodium(I) complex **1a** contains a complete molecular entity in the asymmetric unit, while **2a** crystallizes with an acetone molecule (see Figure 1 for coordination compounds). In both **1a** and **2a**, the rhodium centers are coordinated by the carbonyl and the phosphorus ligands, and the square planar geometry is completed by the bidentate chelating Schiff base ligands 2-(cyclopentyliminomethyl)-5-methylphenolate and 2-(cyclohexyliminomethyl)phenolate for **1a** and **2a**, respectively, forming six-membered chelate rings. The square planar geometry around the metal center in both complexes is distorted as illustrated by the N1-Rh-O1, O1-Rh-C01 and C01-Rh-P angles of 88.16(19), 173.6(2) and 91.7(2)°, respectively, for **1a**, compared with N1-Rh-O1, O1-Rh-C01 and CO1-Rh-P angles of 89.35(17), 175.7(2) and 86.68(19)°, respectively, for **2a**.

The N1-Rh-O1 bite angles formed by the six-membered ring are within normal range and compare well with related structures with bond angles ranging around 87-90° [25]. Other examples of this type of complexes include [Rh(Tfdmaa)(CO)(PPh_3)] (TfdmaaH = l,1,l-trifluoro-5,5-dimethylpentanedione] and [Rh(Sal-NR)(CO)(PPh_3)] (Sal-NRH = N-*o*-tolylsalicylaldiimine) [40,41]. The bite angles in the current Schiff base study are larger than those obtained for the five-membered chelate rings, i.e. [Rh(Ox)(CO)(PPh_3)] (OxH = 8-hydroxyquinoline), [Rh(Trop)(CO)(PR_3)] (TropH = tropolone) and [Rh(Ox)(CO)(DMSO)] (OxH = 8-oxyquinoline)] as well as [Rh(C_9H_7ClNO)(CO)($P(C_6H_4Cl)_3$] (C_9H_7ClNOH = 5-chloro-8-hydroxyquinoline) [42–45], exhibiting bite angles of only 77.38(3) − 81.7(2)°. This can be attributed to the smaller five-membered metal chelate formed compared to the six-membered rings in this study. The Rh-N1 and Rh-O1 bond distances of 2.122(5) and 2.034(5) Å, respectively, for **1a** and 2.091(5) and 2.022(4) Å, respectively, for **2a** are comparable to those found in rhodium(I) complexes with *N,O* donors with bond distances around 2.092(7) − 2.162(4) Å and 2.027(6) − 2.087(4) Å for Rh-N and Rh-O, respectively [34,40,41,46].

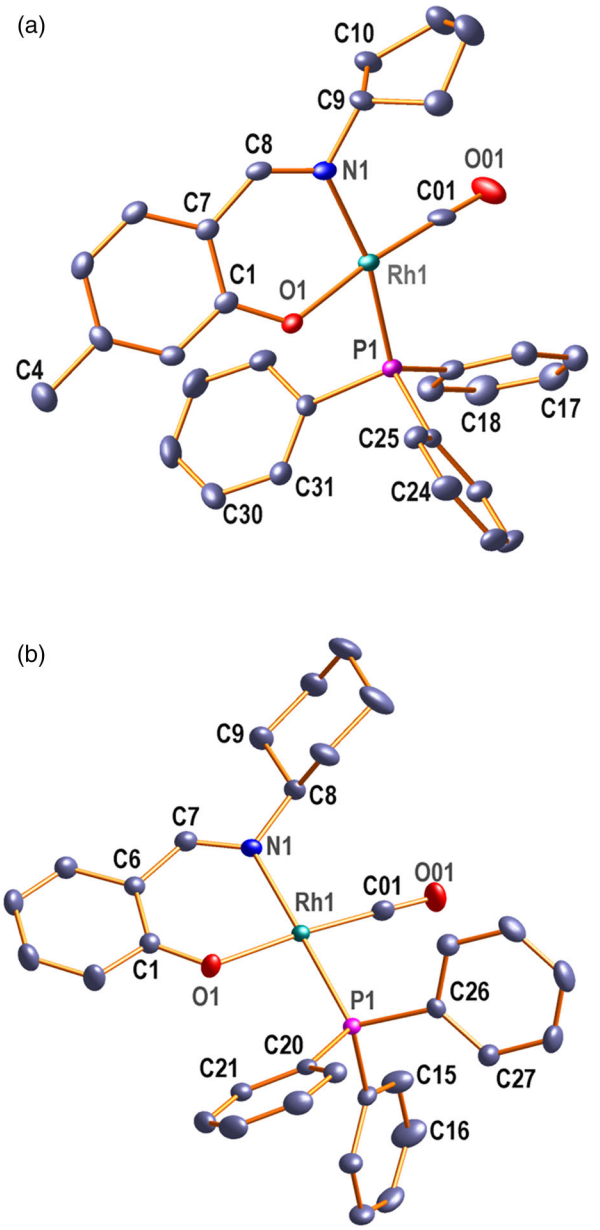

Figure 1. Molecular diagrams (50% probability) of [Rh(5-Me-Sal-CyP)(CO)(PPh_3)] (**1a**) and [Rh(Sal-Cy)(CO)(PPh_3)] (**2a**), showing geometries and atom numbering. Hydrogens and solvent molecules were omitted for clarity.

The rhodium is displaced from the coordination plane by about 0.0389 and 0.005(2) Å for **1a** and **2a**, respectively, with Rh-C01-O01 approximately linear, with reported angles of 178.3(6)° and 178.3(5)° for **1a** and **2a**, respectively. The structure determinations showed that the reaction of the dicarbonyl precursor [Rh(*N,O*-Bid)$(CO)_2$] with PPh_3 leads to the substitution of the carbonyl ligand *trans* to the nitrogen in

Table 2. Selected bond lengths [Å] and angles [°] for **1a** and **2a**.

Bond/Angle	1a	2a
Rh-N1	2.122(5)	2.091(5)
Rh-O1	2.034(5)	2.022(4)
Rh-P	2.2600(16)	2.2798(14)
Rh-C01	1.808(7)	1.810(6)
C01-O01	1.154(8)	1.150(7)
N1-Rh-O1	88.16(19)	89.35(17)
C01-Rh-O1	173.6(2)	175.7(2)
O1-Rh-P	82.25(13)	89.47(12)
P-Rh-N1	168.39(15)	178.53(13)
C01-Rh-N1	98.1(3)	94.5(2)
CO1-Rh-P	91.7(2)	86.68(19)

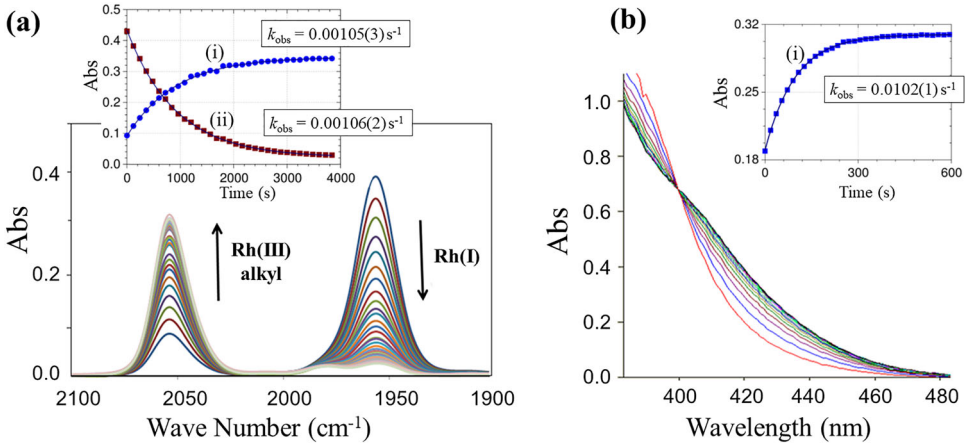

Figure 2. (a) Infrared spectral changes observed during the oxidative addition of MeI to [Rh(5-Me-Sal-CyP)(CO)(PPh_3)] (**1a**) in dichloromethane at 25 °C; insert illustrates (i) the growth of signal from the Rh(III)-alkyl species (k_{obs} = 0.00105(3) s^{-1}); (ii) the disappearance of the Rh(I) reactant (k_{obs} = 0.00106(2) s^{-1}) species. [Rh(5-Me-Sal-CyP)(CO)(PPh_3)] = 9×10^{-3} M, [MeI] = 0.012 M, Δt = 2 min. Solid lines represent the least-squares fit to the usual 1st order exponential [18,47]. (b) Time resolved UV/Vis spectral change for the iodomethane oxidative addition to **1a** in dichloromethane at 25 °C, [Rh] = 3.26×10^{-4} M, [MeI] = 0.12 M, λ = 432 nm, Δt = 20 s, with insert illustrating (i) the absorbance *vs.* time plot [18,47], (k_{obs} = 0.0102(1) s^{-1}).

agreement with the structural *trans* effect (N > O) in both complexes. The Rh-P bond distances of 2.2600(16) Å and 2.2798(14) Å for **1a** and **2a**, respectively, are in agreement with the Rh-P bond lengths found in other *N,O*-Bid complexes with bond distances varying from 2.256(2)-2.81(2) [23,41,42].

2.4. Solution phase study

2.4.1. Preliminary IR, ^{31}P NMR and UV/vis spectroscopy

The reaction progress for iodomethane oxidative addition to the rhodium(I) phosphine complexes [Rh(5-Me-Sal-CyP)(CO)(PPh_3)] (**1a**), [Rh(5-Me-Sal-Cy)(CO)(PPh_3)] (**2a**) and **[**Rh**(**5-Me-Sal-IProp)(CO)(PPh_3)] (**3a**) under pseudo first-order conditions was monitored by IR and UV/visible spectroscopies (Figures 2 and 3). Figure 2(a) presents a series of *in situ* IR spectra obtained for iodomethane oxidative addition to [Rh(5-Me-Sal-CyP)(CO)(PPh_3)] (**1a**),

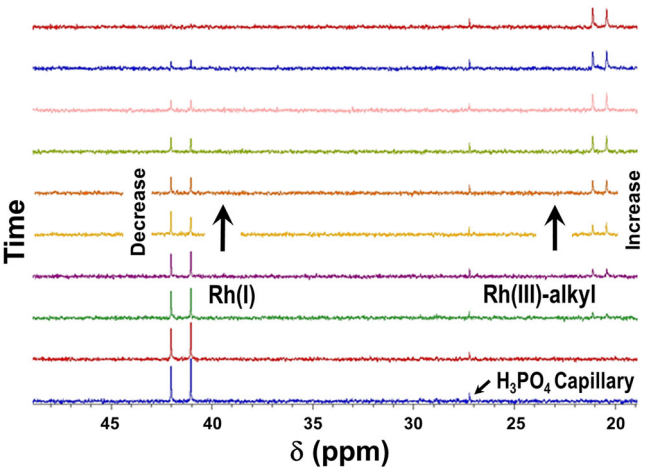

Figure 3. $^{31}P(^{1}H)$-NMR spectra for the disappearance of the Rh(I) complex and the simultaneous formation of the Rh(III)-alkyl species for iodomethane oxidative addition to [Rh(5-Me-Sal-CyP)(CO)(PPh_3)] (**1a**) in dichloromethane at 25 °C; [Rh(I)] = 6×10^{-3} M, [MeI] = 0.06 M, Δt = 2 min, 32 scans per spectrum (referenced to H_3PO_4). Top spectrum collected after 12 h.

forming the Rh(III)-alkyl product, [Rh(5-Me-Sal-CyP)(CO)(Me)(I)(PPh_3)] (**4a**) (Scheme 2). Figure 2(b) illustrates the corresponding UV/vis time-resolved spectra of the reaction.

The successive IR spectra clearly illustrate rapid disappearance of the Rh(I) precursor (ν_{CO} = 1955 cm^{-1}, k_{obs} = $(1.05 \pm 0.03) \times 10^{-3}$ s^{-1}), coupled with simultaneous appearance of a new strong absorption corresponding to Rh(III)-alkyl product at (ν_{CO} = 2054 cm^{-1}, k_{obs} = $(1.06 \pm 0.02) \times 10^{-3}$ s^{-1}).

The observed rate of formation of the Rh(III)-alkyl product is identical to the observed rate for disappearance of the Rh(I) precursor. A notable observation is that *only* the oxidative addition step was observed with no apparent formation of the Rh(III)-acyl, typically resulting from migratory insertion of the coordinated methyl into the Rh-CO bond [18,20]. Also notable is the complete disappearance of the rhodium(I) precursor, indicating a significant forward reaction (large equilibrium constant) with a small reverse reaction. The exclusive formation of the Rh(III)-alkyl product was also confirmed by a time resolved ^{31}P NMR investigation (Figure 3), yielding pseudo first-order rate constants in agreement with those found in both the IR and UV/vis experiments.

The treatment of [Rh(Sal-Cy)(CO)(PPh_3)] (**2a**) or [Rh(5-Me-Sal-IProp)(CO)(PPh_3)] (**3a**) with iodomethane displays the same behavior as **1a**, exclusively forming the Rh(III)-alkyl product with observed pseudo first-order rate constants k_{obs} = 0.00079(2) s^{-1} and 0.00084(2) s^{-1} for the disappearance of the Rh(I) species and k_{obs} = 0.00078(2) s^{-1} and 0.00085(2) s^{-1} for the formation of the Rh(III)-alkyl products **4e** and **4f**, respectively (Scheme 2; Supporting Information).

The observed pseudo first-order rate constants of the oxidative addition are comparable with an increase of about 1.2 times in the order of **1a** > **3a** > **2a**. This result suggests that there is no dramatic effect on the electron density of the rhodium induced by the Schiff base ligands in spite of the variations of the steric and electronic parameters of the ligand backbone: cyclopentyl (**1a**), cyclohexyl (**2a**) and isopropyl (**3a**) groups, respectively, attached to the imine nitrogen. (Both **1a** and **3a** also have

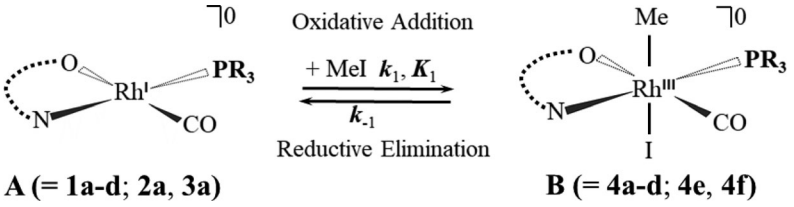

Scheme 2. Iodomethane oxidative addition to [Rh(*N,O*-ScBa)(CO)(PR_3)] complexes (**1a-c**, **2a**, **3a**) {*N,O*-BidH = 5-Me-Sal-CyPH, Sal-CyH, 5-Me-Sal-IPropH (**I-III**)}.

Table 3. A Summary of the rate constants and activation parameters (UV/vis spectroscopy) for the iodomethane oxidative addition to [Rh(N,O-ScBa)(CO)(PPh_3)]; dichloromethane, [Rh] = 3.26×10^{-4} M.

N,O-ScBa =	5-Me-Sal-CyP				Sal-Cy	5-Me-Sal-Iprop
Parameters	**5.1 °C**	**14.9 °C**	**24.3 °C**	**35.2 °C**	**24.8 °C**	**25.1 °C**
10^2 k_1 ($M^{-1}.s^{-1}$)	2.27 ± 0.05	4.11 ± 0.06	7.2 ± 0.2	11.5 ± 0.2	5.3 ± 0.1	5.8 ± 0.1
10^3 k_{-1} (s^{-1})	0.195 ± 0.006	0.49 ± 0.06	1.0 ± 0.2	1.4 ± 0.2	0.2 ± 0.2	0.4 ± 0.2
K_1 (M^{-1})[a]	116 ± 9	84 ± 16	72 ± 15	82 ± 12	26[b]	130[b]
$\Delta H^{\neq}$ (kJ mol^{-1})	–	–	36 ± 1	–	–	–
$\Delta S^{\neq}$ (J K^{-1} mol)	–	–	−145 ± 5	–	–	–

[a]Values should be treated as estimation, as statistical effects are caused by the large standard deviation on the k_{-1} values.
[b]y-intercepts (k_{-1}) even less accurate, resulting in relative e.s.d.'s of >50%.

methyl substituents on the phenolate entity). This is further supported by the first order coupling constant ($^1J_{Rh\text{-}P}$) of the complexes which were 158, 157 and 159 Hz for **1a**, **2a** and **3a**, respectively. The combination of the methyl and cyclopentyl (**1a**), however, introduces the highest, although limited, increased activation. The relative activation by the Schiff base ligands (**I**, **II**, and **III**) is further discussed below.

2.4.2. Kinetic experiments

As indicated above, when **1a-d**, **2a** and **3a** were reacted with iodomethane in dichloromethane under pseudo first-order conditions, *in situ* IR-spectroscopy (Figure 2(a)) showed that the carbonyl band of the reactant at *ca.* 1960 cm^{-1} disappeared, while a new band at *ca.* 2050 cm^{-1} appeared simultaneously. This reaction is also observed by UV/vis spectroscopy (Figure 2(b)) as well as with ^{31}P-NMR spectroscopy (Figure 3). UV/vis experiments were therefore further utilized to study all the variations to complete the study. This reaction is illustrated in Scheme 2, indicating the one-step formation of the Rh^{III}-alkyl species **B** (**4a-c**, **4e**, **4f**), since no tendency of rhodium(III)-acyl formation was observed after > 12 h (Figure 3), more than 10 h after the alkyl species formed completely.

As indicated, the UV/visible kinetic data obtained for the iodomethane oxidative addition to [Rh(5-Me-Sal-CyP)(CO)(PPh_3)] (**1a**), [Rh(Sal-Cy)(CO)(PPh_3)] (**2a**) and [Rh(5-Me-Sal-IProp)(CO)(PPh_3)] (**3a**) correspond very well to those obtained from the IR and ^{31}P NMR spectroscopy results. A summary of the data obtained for these reactions is presented in Table 3, and plots of the observed first-order rate constants k_{obs} *vs.* iodomethane concentration all show a linear dependency on the [MeI], as predicted by Eq. 1 and illustrated previously [18] (Figure 4).

$$k_{obs} = k_1[MeI] + k_{-1} \quad (1)$$

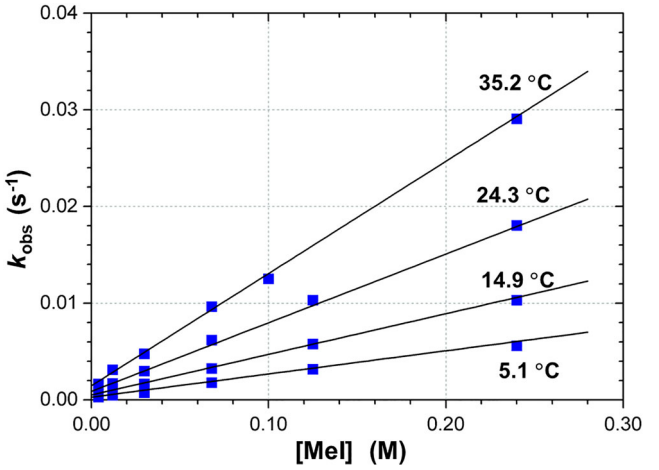

Figure 4. Plots of the observed rate constants (k_{obs}) *vs.* iodomethane concentrations for iodomethane oxidative addition to [Rh(5-Me-Sal-CyP)(CO)(PPh_3)] at various temperatures; [Rh] = 3.26×10^{-4} M, $\lambda = 432$ nm. The lines represent the simultaneous global fit of the data to Eq. 1 and the Eyring equation [18,48].

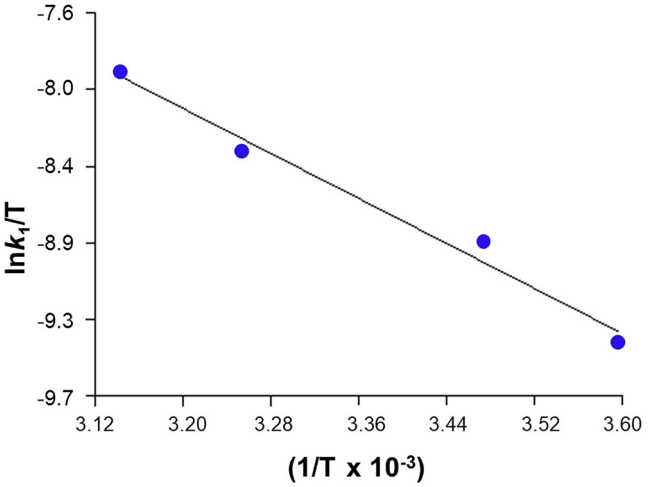

Figure 5. Eyring plot of the second order rate constants (k_1) for the formation of [Rh(5-Me-Sal-CyP)(CH_3)(I)(CO)(PPh_3)] in dichloromethane.

The relatively small intercepts (*ca.* zero within most e.s.d.'s) for the reverse reaction (k_{-1}) values obtained supports the proposed direct mechanism with no solvent dependent pathway. This is further evidenced by the IR study, indicating a large equilibrium constant as denoted by K_1 in Scheme 2.

A temperature variation study (Figure 4) was conducted for the iodomethane oxidative addition to [Rh(5-Me-Sal-CyP)(CO)(PPh_3)] (**1a**) to enable determination of the activation parameters from which an Eyring plot (Figure 5) was obtained. In Figure 4, the solid lines represent the least-squares fits of k_{obs} vs. [MeI] at different temperatures, consistent with the rate expressed in Eq. 1. A summary of the data obtained is given

Table 4. A Summary of the rate constants for the iodomethane oxidative addition to [Rh(L,L'-Bid)(CO)(PR_3)] (PR_3 = PPh_3, PPh_2Cy, $PPhCy_2$ and PCy_3) at 25 °C in dichloromethane. L,L'-Bid represents four different ligand systems, where N,O-BidH is 5-Me-Sal-CyP (six-membered chelates) or 8-hydroxyquinoline (N,O-Ox; five-membered chelates), O,O-BidH = acetylacetone (six-membered chelates), and S,O-BidH = N-benzoyl-N',N'-diphenylthiourea (six-membered chelates).

PR_3	ν_{CO} (cm^{-1})	δ ^{31}P (ppm)	$^1J_{Rh-P}$ (Hz)	Cone[b] angle (°)	pK_a[c] free phosphine	O-Rh-N (°)	O–N (Å)	10^3 k_1[d] ($M^{-1}s^{-1}$)	10^3 k_{-1} (s^{-1})	K_1 (M^{-1})	$\Delta H^{\neq}$ (kJ/mol)	$\Delta S^{\neq}$ (J/K.mol)
[Rh(***5-Me-Sal-CyP***)(CO)(PR_3)][a]												
PPh_3	1955	42	158	145	3.28	88.1(1)	2.885(4)	72 ± 2	1.0 ± 0.02	72 ± 5	36 ± 1	−145 ± 5
$PCyPh_2$	1945	50	156	153	5.87	–	–	146 ± 1	1.47 ± 0.02	99 ± 2	–	–
PCy_2Ph	1943	54	156	–	8.46	–	–	21 ± 2	0.71 ± 0.05	37 ± 7	–	–
PCy_3	1937	50	151	156	11.3	–	–	82 ± 1	2.1 ± 0.1	39 ± 4	–	–
[Rh(***N,O-Ox***)(CO)(PR_3)][e]												
PPh_3	1965	41	164	156	3.28	79.41(9)	2.676(3)	39 ± 1	<0.1	>400	58.9 ± 0.2	−74.1 ± 0.06
$PCyPh_2$	1968	52	163	151	5.87	–	–	86 ± 2	<0.1	>400	–	–
PCy_2Ph	1952	54	161	–	8.46	–	–	8 ± 1	<0.01	>400	–	–
PCy_3	1946	55	156	167	11.3	80.64(15)	2.671(5)	28 ± 1	<0.1	>400	–	–
[Rh(***O,O-acac***)(CO)(PR_3)][f]												
PPh_3	1978	49	177	149	3.28	88.02(6)	2.854(3)	30.8 ± 0.5	1.1 ± 0.2	27 ± 4	38 ± 1	−146 ± 4
$PCyPh_2$	1959	53	171	151	5.87	88.71(7)	2.880(3)	55 ± 1	0.9 ± 0.4	59 ± 26	35 ± 3	−152 ± 9
PCy_2Ph	1949	59	168	164	8.46	88.19(6)	2.867(2)	7.0 ± 1	0.08 ± 0.02	90 ± 24	44 ± 1	−140 ± 5
PCy_3	1945	59	164	170	11.3	87.78(4)	2.866(2)	27.1 ± 0.2	0.29 ± 0.09	92 ± 29	36 ± 3	−154 ± 9
[Rh(***S,O-BdiPT***)(CO)(PR_3)][e]												
PPh_3	1979	38	152	145	3.28	91.4(1)	3.115(4)	5.1 ± 0.3[g]	>100	<0.05	42 ± 2	−147 ± 7
$PCyPh_2$	1972	45	149	153	5.87	91.09(7)	3.111(2)	6.4 ± 0.3[g]	>100	<0.05	42 ± 1	−146 ± 3
PCy_2Ph	1969	49	149	–	8.46	–	–	0.82 ± 0.08[g]	>100	<0.05	48 ± 1	−144 ± 4
PCy_3	1963	50	146	156	11.3	91.73(9)	3.154(3)	2.8 ± 0.02[g]	>100	<0.05	46 ± 2	−140 ± 6

[a]This work.
[b]Calculated from solid state data; Ref. 18.
[c]Obtained from Ref. 39.
[d]Calculated from figures 4 and 6 using Eq. 1.
[e]Ref. 23.
[f]Ref. 18.
[g]Represent formation of the acyl species via the alkyl, where $k'_2 = k_{ac}K_1[MeI]/(1 + K_1[MeI]) \approx k_{ac}K_1[MeI]$ (when $K_1[MeI] \ll 1$; k_{ac} = conversion of alkyl into acyl species).

in Table 3. Virtually identical values for the activation parameters were obtained from a global fit, as described previously [48].

The values obtained for the activation parameters, $\Delta H^{\neq} = 36 \pm 1$ kJ mol^{-1} and $\Delta S^{\neq} = -145 \pm 5$ (J K^{-1} mol), are characteristic of an *associative* type mechanism for the formation of the Rh(III)-alkyl product [22,23,25], where the attack by the electron rich Rh(I) center on the iodomethane substrate is the driving force for the reaction.

A summary of the data, illustrating the relative dependence of the rate constants on the Schiff bases and the tertiary phosphine ligands, is given in Figure 6 and reported in Tables 3 and 4. Figure 6(a) illustrates the relative (small) effect of the three *N,O*-ScBa ligands **I**, **II** and **III** on the iodomethane oxidative addition rates, and as indicated above, the combination of the methyl and cyclopentyl substituents in **1a** induces the most activation, albeit only about 1.2 times compared to **2a** and **3a**.

Since rhodium(I) acts as a nucleophile in the oxidative addition reaction, naturally one expects an increase in activation of the metal center towards oxidative addition when replacing weaker electron-donating phenyl rings on the phosphine ligands with more electron-rich cyclohexyl rings. However, the results obtained for the various phosphine ligands suggest otherwise. It is clear from Figure 6(b) and Table 4 that a relative reactivity in the iodomethane oxidative addition is observed in the order [Rh(5-Me-SalCyP)(CO)(PPh_2Cy)] (**1 b**) > [Rh(5-Me-SalCyP)(CO)(PCy_3)] (**1d**) > [Rh(5-Me-SalCyP)(CO)(PPh_3)] (**1a**) > [Rh(5-Me-SalCyP)(CO)($PPhCy_2$)] (**1c**).

The treatment of these rhodium(I) complexes with iodomethane shows a clean and direct conversion of the rhodium(I) precursor to the rhodium(III) alkyl species as the final product. Thus, there is no apparent formation of the acyl product observed for all the rhodium(I) complexes, as indicated by the IR and ^{31}P NMR data [18,25]. In the current case, the substituent on the N atom in the series of *N,O*-ScBaH ligands (CyP, Cy and IProp) seemingly exhibits a subtle (responsive) steric effect. The assumed *trans* coordination of the methyl and the iodide, following the two-electron transfer from Rh(I), only yields an octahedral *trans* oxidative addition Rh^{III}-alkyl product (**4a**-**4f** in Scheme 2). Although reasonably well favored thermodynamically, the [Rh^{III}(5-Me-SalCyP)(CO)(Me)(I)(PR_3)] products do not allow methyl migration to the coordinated CO, and the reaction is effectively stopped at the alkyl species [18,25].

Moreover, as illustrated, even if the substituent on the N-atom was varied as three aliphatic substituents {cyclopentyl (CyP), cyclohexyl (Cy) and isopropyl (IProp)}, it is clear that conditions have been achieved wherein still *only* the subtle intermediate stereo-electronic requirements for the Rh^{III}-alkyl species are met. Thus, the *total* oxidative addition is not blocked, nor is the Rh^{III}-alkyl species bottlenecked, to allow the Rh^{III}-acyl species to form as in examples above and in the literature [49–51]. The Schiff base ligands described herein therefore seemingly have just the correct steric demand to *allow* alkyl formation (fairly ideal octahedral complex), but *not* the methyl migraton, which, in spite of being only five-coordinate, requires in the Schiff base systems more steric demand at the *acetyl site*. Thus, although the acetyl complexes adopt a square pyramidal geometry, the much more bulky acetyl entity on one side of the Rh(III) is seemingly thermodynamically less favorable than the *trans* Me-Rh^{III}-I orientation, having a methyl substituent on the one side and an iodido ligand on the other. The steric demand of the apical site (formation of the acyl complex) is augmented by the fact that the iodido ligand moves to the square plane, increasing the

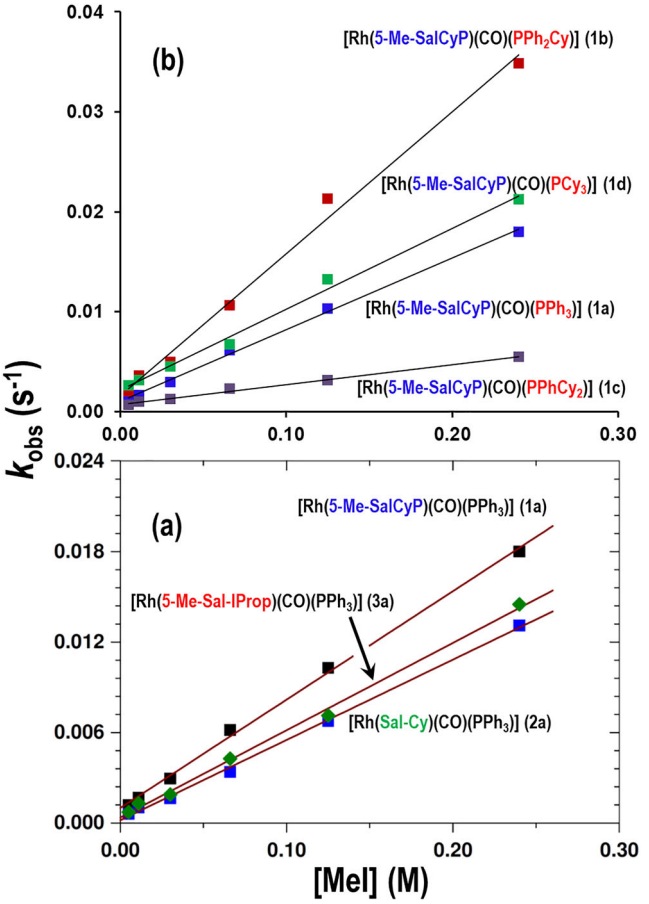

Figure 6. Effect of (a) the *N,O*-ScBa ligands in [Rh(*N,O*-ScBa)(CO)(PPh_3)] (**1a**, **2a**, **3a**) and (b) the tertiary phosphine ligands in [Rh(5-Me-Sal-CyP)(CO)(PR_3)] (PR_3 = PPh_3, PPh_2Cy, $PPhCy_2$ and PCy_3, **1a-d**); on the observed rate constant, k_{obs}, for the iodomethane oxidative addition in dichloromethane at 25 °C using the UV/Vis spectroscopy. [Rh] = 3×10^{-4} M, $\lambda = 432$ nm.

overall steric demand at the acetyl-entity site. The octahedral six-coordinate geometry of the alkyl species (**4a**-**4f**) is therefore thermodynamically more favored in the current study than the five-coordinate square pyramidal acetyl final product.

2.5. General correlation of [Rh(L,L'-Bid)(CO)(PR_3)] complexes

The results obtained from this study may be correlated with similar isostructural Rh(I) complexes reported in literature (see Table 4 and Figure 7). Thus, [Rh(*L,L'*-Bid)(CO)(PR_3)] complexes (PR_3 = PPh_3, PPh_2Cy, $PPhCy_2$ and PCy_3) are presented wherein *L,L'*-Bid represents four different ligand systems, with varying N, O and S donor atom combinations within the chelating moiety:

a. *N,O*-BidH representing (i) 5-Me-Sal-CyP (six-membered *Schiff base* chelates; this study) and (ii) 8-hydroxyquinoline (*N,O*-Ox; five-membered chelates);
b. *O,O*-BidH = acetylacetone (six-membered chelates);
c. *S,O*-BidH = *N*-benzoyl-*N'*,*N'*-diphenylthiourea (six-membered chelates).

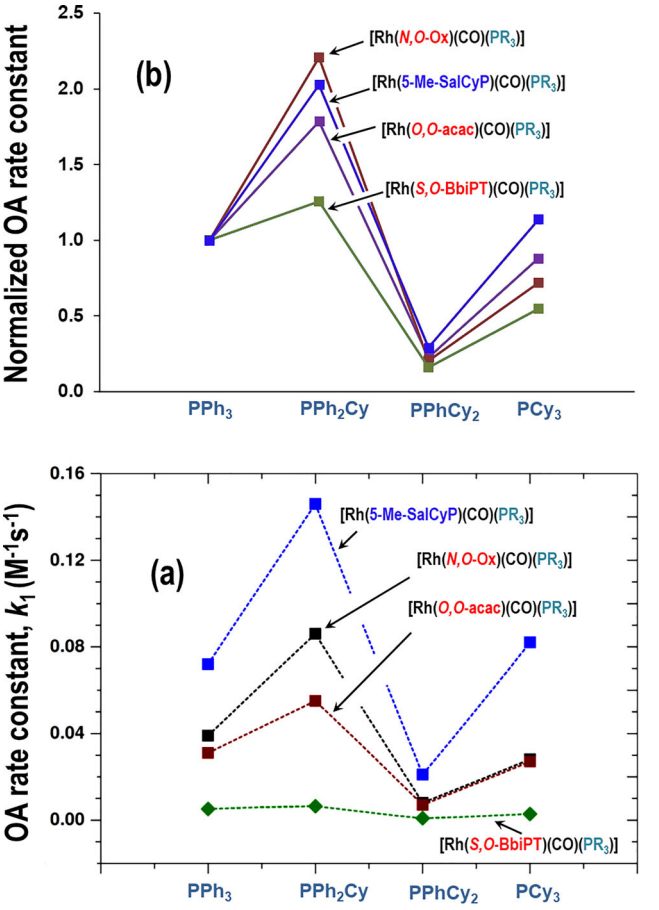

Figure 7. Relative rate constants of the iodomethane oxidative addition (OA) to different [Rh(*L*,*L*′-Bid)(CO)(PR_3)] complexes, illustrating [Rh(5-Me-SalCyP)(CO)(PR_3)], [Rh(*N*,*O*-Ox)(CO)(PR_3)], [Rh(*O*,*O*-acac)(CO)(PR_3)] and [Rh(*S*,*O*-BbiPT)(CO)(PR_3)] where R = Ph or Cy, at 25 °C. (a) *Direct* second order oxidative addition rate constants. (b) *Normalized* 2nd order oxidative addition rate constants [relative to PPh_3=1] of complexes.

The relative influence of the combined *L*,*L*′-Bid bidentate ligands (O, N, S donor atoms) and PR_3 as illustrated in Figure 7 (data in Table 4) for all four types of *L*,*L*′-Bid bidentate ligands given above shows a similar, interesting phenomenon. The observed iodomethane oxidative addition rates are presented as (i) *direct* 2nd order rate constants (Figure 7(a)) as well as (ii) the '*normalised*' relationship (considering PPh_3 = 1), Figure 7(b), for all the [Rh(*L*,*L*′-Bid)(CO)(PR_3)] complexes. Surprisingly, it follows exactly the same relative profile, albeit that there is an approximate *two* order-of-magnitude overall difference in reactivity (Figure 7(a)) for the four types of bidentate ligands given in points (a)-(c) above. It underlines the similar adaptive nature of the four PR_3 ligands utilized and indicates a subtle interplay between the steric and electronic parameters operative in these complexes, independent of donor atoms or bidentate bite angles. Moreover, it suggests a responsive effect within the tertiary phosphine ligands, allowing them to self-adjust depending on the substituents and bidentate ligand(s).

The rates of the oxidative addition obtained for [Rh(*N,O*-Bid)(CO)(PR_3)] with iodomethane appear to be generally faster than those of the corresponding [Rh(*O,O*-Bid)(CO)(PR_3)] (OxH = oxine) and the [Rh(*S,O*-Bid)(CO)(PPh_3)] complexes. The *S,O*-Bid complexes clearly show a much larger relative influence by the bulkier thioureato ligand (larger chelate bite angle) compared to the acac, oxine and Schiff bases. Moreover, as emphasized in Figure 7(b), all four *L,L'*-Bid ligand system complexes exhibit exactly the same relative behavior, indicating that the PPh_2Cy complex is significantly activated, while the $PPhCy_2$ is inhibiting the oxidative addition the most. Assuming it to be a steric effect, it means that the $PPhCy_2$ surprisingly generates *'in situ'* a much larger apparent steric effect than even the PCy_3 ligand, independent of the bidentate ligand present.

Indeed, the delicate interplay between the Rh^{III}-alkyl species and the Rh^{III}-acyl species may thus be manipulated with a combined *N,O*-ScBa/PR_3 ligand configuration that creates a *responsive* self-adjusting system which selectively allows formation of the Rh^{III}-alkyl species, yet blocking the formation of the Rh^{III}-acyl species. In principle it may be considered as a chemical speciation probe or for that matter, a *sensor* for MeI in a responsive environment.

3. Conclusion

The synthesis and characterization of a series of [Rh(*N,O*-ScBa)(CO)(PR_3)] (PR_3 = PPh_3, PPh_2Cy, $PPhCy_2$ and PCy_3) complexes (*N,O*-ScBaH = Schiff bases) including two crystal structure determinations (**1a** and **2a**) were performed, followed by a detailed mechanistic investigation into the iodomethane oxidative addition thereto. The iodomethane oxidative addition, typically proceeding via an associatively activated mechanism (large negative $\Delta S^{\neq}$ values) is accepted to be due to the electron-rich Rh(I) metal center acting as nucleophile. It is manifested in a relatively fast equilibrium for the oxidative addition/reductive elimination in the range of [Rh(5-Me-SalCyP)(CO)(PR_3)] (R = phenyl or cyclohexyl) complexes (**1a**-**d**), as well as to [Rh(Sal-Cy)(CO)(PPh_3)] (**2a**) and [Rh(5-Me-Sal-IProp)(CO)(PPh_3)] (**3a**). The reaction was well-defined for all complexes, leading *exclusively* to formation of the octahedral Rh^{III}-alkyl species, [Rh(*N,O*-ScBa)(CO)(Me)(I)(PR_3)] as final products. The reason for this lies in the subtle steric effect exerted primarily by the *N,O*-ScBa ligand, whereupon the tertiary phosphine ligands adjust themselves to accommodate the alkyl formation, yet does *not* allow the further migratory insertion to produce the square pyramidal Rh^{III}-acyl species [Rh(*N,O*-ScBa)(COMe)(I)(PR_3)].

Oxidative addition rates for the different Schiff base complexes (**1a**, **2a**, **3a**) showed only a factor of 1.2 variation, indicating that the substituents on the periphery of the ScBaH ligands were stereo-electronically very similar and did not significantly affect the electron density at the metal center.

In the case of the [Rh(5-Me-SalCyP)(CO)(PR_3)] complexes, a significant *relative* effect of the oxidative addition rate on the tertiary phosphine (about *one* order-of-magnitude) was observed, with the $PPhCy_2$ complex the slowest, the PPh_2Cy the most rapid, and the PPh_3 and PCy_3 lying between the mentioned first two. This is neither in agreement with the expected electron density induced by the tertiary phosphine, nor with

the cone angles of the phoshine ligands. Yet, it confirms the consistent behavior of the four PR_3 ligands as found for three other bidentate ligand complex systems from literature, i.e. [Rh(*N,O*-Ox)(CO)(PR_3)], [Rh(*O,O*-acac)(CO)(PR_3)] and [Rh(*S,O*-BbiPT)(CO)(PR_3)] (Table 4; Figure 7) where R = Ph or Cy, displaying the unexpected relative reactivity relationship.

In the *N,O*-ScBaH ligands described herein, three things stand out. First, the combination of them and the PPh_3, PPh_2Cy, $PPhCy_2$ and PCy_3 allows a *responsive* system which totally inhibits the formation of the final Rh^{III}-acyl species usually encountered. Second, ScBaH introduces significantly more electron density (clearly manifested in the *increased* relative oxidative addition rates, even compared for example to the *S,O*-Bid ligands described above) to the metal center by the softer nature of the net *N,O*-donor atom combination, coupled with the more *ideal* bite angle enforced by the Schiff bases. Third, the increased reactivity is manifested in the relative rates of oxidative addition, placing the *N,O*-ScBa systems at the top and even *two* orders-of-magnitude larger than the S,O-Bid ligand systems of thioacetylacetone or thiourea.

4. Experimental

4.1. General procedure and instrumentation

All the reagents used were of analytical reagent grade, purchased from Sigma-Aldrich, South Africa and were used as purchased without purification. The ^{13}C and ^{1}H NMR spectra of the ligands and metal complexes were recorded at 75.48 and 300.13 MHz, respectively, on a Bruker AXS 300 MHz or on a Bruker AXS 400 MHz (100.61 and 400.13 MHz, respectively). ^{1}H NMR data are listed in order: chemical shift (δ) reported in ppm and referenced to the solvent peak, multiplicity, coupling constant (*J*, in Hz), number of hydrogens, assignment. Hydrogen and carbon decoupled experiments ^{31}P NMR spectra were recorded on a 400 MHz Bruker spectrometer operating at the ^{31}P frequency of 161.98 MHz (2074 scans, pulse of 30° and delay time of 1.89 s). The ^{31}P NMR data are reported in the order: chemical shift (δ) reported in ppm and referenced to H_3PO_4 capillary, multiplicity, number of phosphorus atoms, coupling constants (*J* in Hz).

4.2. Ligands synthesis

4.2.1. Synthesis of 5-Me-Sal-CyPH (I)

Cyclopentylamine (0.313 g, 3.676×10^{-3} mol) was added dropwise to 2-hydroxy-4-methylbenzaldehyde (0.500 g, 3.672×10^{-3} mol) in methanol (20 ml). The solution was heated at 80 °C for 3 h. Removal of the solvent under vacuum afforded the product as a yellow powder (yield: 0.697 g, 93.4%). ^{1}H NMR (300 MHz, MeOD) δ 8.35 (s, 1H), 7.15 (s, 1H), 6.63 (s, 2H), 3.87 (s, 1H), 2.28 (s, 3H), 2.11 – 1.56 (m, 8H). ^{13}C NMR (101 MHz, Methanol-d_4) δ 165.09, 162.91, 144.25, 131.54, 118.48, 117.92 115.56 (Ar), 67.59 (CH), 34.11, 23.68 (CH_2), 20.50 (CH_3).

4.2.2. Synthesis of Sal-CyH (II)

Cyclohexylamine (0.86 g, 8.847×10^{-3} mol) was dissolved in 2 ml methanol and the solution was added dropwise to salicylaldehyde (1.15 g, 9.412×10^{-3} mol) in methanol (20 ml). Anhydrous $MgSO_4$ was added and the solution heated at 80 °C for 3 h. $MgSO_4$ was filtered off and the solvent was removed under reduced pressure, yellow oil was obtained which was dissolved in acetone to crystallize (yield: 1.278 g, 70.8%). ^{1}H NMR (300 MHz, MeOD) δ 8.41 (s, 1H), 7.29 (s, 2H), 6.85 (s, 2H), 1.22 (s, 11H). ^{13}C NMR (101 MHz, Acetone-d_6) δ 166.49, 166.25, 145.65, 132.94, 119.88, 119.32, 116.42 (Ar), 35.15, 34.12, 33.13, 25, 15, 24.12, 18.21 (Cy).

4.2.3. Synthesis of 5-Me-Sal-IPropH (III)

Isopropylamine (0.228 g, 3.857×10^{-3} mol) was added dropwise to 2-hydroxy-4-methyl-benzaldehyde (0.501 g, 3.680×10^{-3} mol) in methanol (20 ml). The solution was heated at 80 °C for 3 h. The solvent was removed under reduced pressure resulting in a yellow powder (yield: 0.582 g, 89.2%). ^{1}H NMR (300 MHz, CD_2Cl_2) δ 8.25 (s, 1H), 7.17 (s, 1H), 6.81 (s, 1H), 6.55 (s, 1H), 4.30 (s, 1H), 2.32 (s, 3H), 1.53 (s, 6H). ^{13}C NMR (101 MHz, $CDCl_3$) δ 161.69, 161.51, 142.88, 130.90, 119.49, 117.44, 116.44 (Ar), 59.81 (CH), 24.23 ($2 \times CH_3$), 21.39 (CH_3).

4.3. General synthesis of the rhodium(I) monophosphine complexes

The monophosphine complexes, [Rh(*N,O*-ScBa)(CO)(PR_3)], were prepared by dissolving the dicarbonyl complexes [18] in a minimum of acetone followed by addition of the tertiary phosphine ligand PR_3 as previously reported (Scheme 3). Due to the large *trans* influence of the N-atom and the corresponding thermodynamic stability only Isomer A was obtained.

4.3.1. Synthesis [Rh(5-Me-Sal-CyP)$(CO)_2$] (1)

$RhCl_3 \cdot xH_2O$ (0.021 g, 0.079 mmol) was dissolved in 5 ml of DMF and refluxed until the red color turned yellow (approx. 30 min). 2-(Cyclopentyliminomethyl)-5-methylphenol = 5-Me-Sal-CyPH (0.019 g, 0.095 mmol) was added to the cooled solution of [Rh(μ-Cl)$(CO)_2]_2$. After two minutes of stirring, the product was precipitated by ice water and isolated by centrifugation. The product was recrystallized by dissolving it in 1 ml acetone and allowing slow evaporation (yield: 0.024 g, 80%). IR (ATR): ν_{CO} = 2067, 1987 cm^{-1}. ^{1}H NMR (400 MHz, CD_3CN) δ 8.33 (s, 1H, HC = N), 7.25 (s, 1H), 6.72 (s, 1H), 6.54 (s, 1H), 3.87 (m, 1H), 2.27 (s, 3H), 1.89-1.23 (m, 8H, Cyp). ^{1}H NMR (400 MHz, CD_3CN) δ 8.37 (s, 1H), 7.34 (s, 2H), 6.86 (s, 1H), 6.68 (s, 1H), 3.88 (s, 1H), 2.26 – 2.17 (m, 2H), 1.87 (s, 1H), 1.75 (d, J = 4.9 Hz, 3H), 1.48 – 1.34 (m, 2H), 1.16 (d, J = 20.6 Hz, 1H). ^{13}C NMR (101 MHz, DMSO) δ 166.09, 162.91, 144.25, 131.45, 118.48, 117.92, 115.56 (Ar), 67.59 (CH), 34.11, 23.68, 20.50 (cyclopentyl).

4.3.2. Synthesis of [Rh(Sal-Cy)$(CO)_2$] (2)

$RhCl_3 \cdot xH_2O$ (0.020 g, 0.076 mmol) was dissolved in 5 ml of DMF and the solution was refluxed for approximately 30 minutes. The solution was cooled and 2-(cyclohexyliminomethyl)phenol = SalH-Cy (0.019 g, 0.091 mmol) was added to the

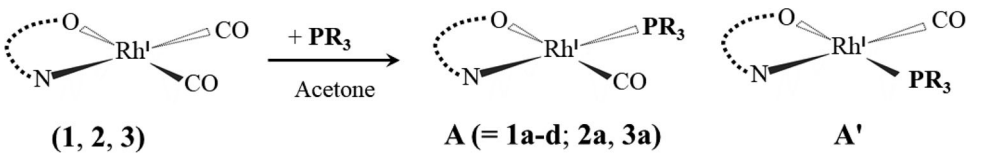

Scheme 3. General synthesis of the rhodium(I) monophosphine complexes [Rh(*N,O*-ScBa)(CO)(PR_3)].

cooled reaction mixture. After two minutes of stirring, the product was precipitated by ice water and isolated by centrifugation. The product was recrystallized by dissolving it in 1 ml acetone and allowing slow evaporation (yield: 0.018 g, 64%). IR (ATR): ν_{CO} 2052, 1982 cm^{-1}. ^1H NMR (400 MHz, CD_3CN) δ 8.37 (s, 1H, HC = N), 7.34 (s, 2H), 6.86 (s, 1H), 6.68 (s, 1H), 3.88 (m, 1H), 1.87-1.13 (m, 10H, Cyc). ^1H NMR (300 MHz, CD_2Cl_2) δ 8.21 (s, 2H), 7.13 (s, 2H), 6.77 (s, 2H), 6.51 (s, 2H), 4.26 (s, 2H), 2.28 (s, 6H), 1.42 (s, 13H). ^{13}C NMR (101 MHz, DMSO) δ 166.49, 164.31, 145.65, 133.94, 119.88, 119.32 116.96 (Ar), 69.89 (CH), 35.51, 25.08, 21.90 (cyclohexyl).

4.3.3. Synthesis of [Rh(5-Me-Sal-IProp)(CO)$_2$] (3)

$RhCl_3 \cdot xH_2O$ (0.020 g, 0.076 mmol) was dissolved in 5 ml of DMF and the solution was refluxed for approximately 30 minutes. The solution was cooled and then 5-methyl-2-(isopropyliminomethyl)phenol = 5-Me-Sal-IPropH (0.016 g, 0091 mmol) was added to the reaction mixture and stirred. After two minutes of stirring, the product was precipitated by ice water and isolated by centrifugation. The product was recrystallized by dissolving it in 1 ml acetone and allowing slow evaporation (yield: 0.016 g, 63%). IR (ATR): ν_{CO} 2062, 1994 cm^{-1}. ^1H NMR (300 MHz, CD_2Cl_2) δ 8.22 (s, 1H, Ar), 7.16 (s, 1H, Ar), 6.78 (s, 1H, Ar), 6.54 (s, 1H, Ar), 4.26 (s, 1H, CH), 2.28 (s, 3H, CH_3), 1.4 (s, 6H, $2 \times CH_3$). ^1H NMR (400 MHz, CD_3CN) δ 7.28 − 7.24 (m, 4H), 6.73 − 6.71 (m, 4H), 6.57 − 6.52 (m, 4H), 4.34 − 4.23 (m, 2H), 2.27 (s, 6H), 1.94 (dt, $J = 4.9$, 2.5 Hz, 28H), 1.49 (d, $J = 6.6$ Hz, 24H), 1.30 − 1.22 (m, 5H). ^{13}C NMR (101 MHz, DMSO) δ 161.69, 161.51, 142.88, 130.90, 119.49 117.44, 116.44 (Ar), 59.81(CH), 24.23 ($2 \times CH_3$), 21.29 (CH_3).

4.3.4. Synthesis of [Rh(5-Me-Sal-CyP)(CO)(PPh$_3$)] (1a)

[Rh(5-Me-Sal-CyP)$(CO)_2$] (0.040 g, 0.067 mmol) was dissolved in 2 ml acetone to which PPh_3 (0.01 g, 0.080 mmol) was added. The solvent was allowed to evaporate slowly resulting in a yellow product (yield: 0.039 g, 59%). IR (ATR): ν_{CO} 1955 cm^{-1}; UV/Vis (nm, $mol^{-1}\,cm^{-1}$): λ_{max} = 394 nm, ε = 2856; $^{31}P\{^1H\}$(161.0 MHz, DMSO) δ = 41.5 (d, $^1J_{Rh\text{-}P}$ = 158 Hz) ppm. ^1H NMR (400 MHz, Acetone) δ 8.49 (s,1H), 7.7 (s, 6H), 7.48 (s, 9H), 7.0 (s, 1H), 6.33 (s, 1H), 6.09 (s, 1H), 4.36 (s, 1H), 1.55 (s, $2 \times CH_3$).

4.3.5. Synthesis of [Rh(5-Me-Sal-CyP)(CO)(PPh$_2$Cy)] (1b)

[Rh(5-Me-Sal-CyP)$(CO)_2$] (0.041 g, 0.068 mmol) was dissolved in 2 ml acetone to which PPh_2Cy (0.022 g, 0.081 mmol) was added. The solvent was allowed to evaporate slowly resulting in a yellow product (yield: 0.038 g, 56%). IR (ATR): ν_{CO} 1945 cm^{-1}; UV/Vis (nm, $mol^{-1}\,cm^{-1}$): λ_{max} = 391 nm, ε = 2564; $^{31}P\{^1H\}$(161.0 MHz, DMSO) δ = 49.5 (d, $^1J_{Rh\text{-}P}$ = 156 Hz) ppm. ^1H NMR (400 MHz, Acetone) δ 8.43 (s,1H), 7.79 (m, 10H), 7.15 (s, 1H), 6.42 (s, 1H), 6.34 (s, 1H), 4.40 (m, 1H), 1.89-1.61 (m, 10H), 1.57-1.23 (m 10H).

4.3.6. Synthesis of [Rh(5-Me-Sal-CyP)(CO)(PPhCy$_2$)] (1c)

[Rh(5-Me-Sal-CyP)(CO)$_2$] (0.042 g, 0.069 mmol) was dissolved in 2 ml acetone to which PPhCy$_2$ (0.023 g, 0.083 mmol) was added. The solvent was allowed to evaporate slowly resulting in a yellow product (yield: 0.031 g, 44%). IR (ATR): ν_{CO} 1943 cm^{-1}; UV/Vis (nm, mol^{-1} cm^{-1}): λ_{max} = 390 nm, ε = 2678; $^{31}P\{^1H\}$(161.0 MHz, DMSO) δ = 53.8 (d, $^1J_{Rh\text{-}P}$ = 155 Hz) ppm. ^{1}H NMR (400 MHz, Acetone) δ 8.45 (s, 1H), 7.89 (s, 2H), 7.49 (s, 3H), 7.17 (s, 1H), 6.48 (s, 1H), 6.35 (s,1H), 4.46 (s,1H), 1.9-1.81 (m 9H), 1.74-1.10 (m, 22 H).

4.3.7. Synthesis of [Rh(5-Me-Sal-CyP)(CO)(PCy$_3$)] (1d)

[Rh(5-Me-Sal-CyP)(CO)$_2$] (0.040 g, 0.065 mmol) was dissolved in 2 ml acetone to which PCy$_3$ (0.022 g, 0.078 mmol) was added. The solvent was allowed to evaporate slowly resulting in a yellow product (yield: 0.043 g, 63%). IR (ATR): ν_{CO} 1937 cm^{-1}; UV/Vis (nm, mol^{-1} cm^{-1}): λ_{max} = 391 nm, ε = 2671; $^{31}P\{^1H\}$(161.0 MHz, DMSO) δ = 50.2(d, $^1J_{Rh\text{-}P}$ = 151 Hz) ppm. ^{1}H NMR (400 MHz, Acetone) δ 8.45 (s,1H), 7.89 (s, 1H), 6.58 (s, 1H), 6.33 (s, 1H), 4.44 (m, 1H), 2.44 (s, 3H), 1.95-1.78 (m, 9H), 1.65-1.25 (m, 33H).

4.3.8. Synthesis of [Rh(Sal-Cy)(CO)(PPh$_3$)] (2a)

[Rh(Sal-Cy)(CO)$_2$] (0.044 g, 0.12 mmol) was dissolved in 2 ml acetone to which PPh$_3$ (0.032 g, 0.15 mmol) was added. The solvent was allowed to evaporate slowly resulting in a yellow product (yield: 0.048 g, 43%). IR (ATR): ν_{CO} 1957 cm^{-1}; UV/Vis (nm, mol^{-1} cm^{-1}): λ_{max} = 388 nm, ε = 2453; $^{31}P\{^1H\}$(161.0 MHz, DMSO) δ = 41.6 (d, $^1J_{Rh\text{-}P}$ = 158 Hz) ppm. ^{1}H NMR (400 MHz, DMSO) δ 8.56 (s, 1H), 7.73 – 7.38 (m, 15H), 7.09 (s, 1H), 6.87 (s, 1H), 6.49 (s, 1H), 6.09 (s, 1H), 2.29-1.08 (m, 11H).

4.3.9. Synthesis of [Rh(5-Me-Sal-IProp)(CO)(PPh$_3$)] (3a)

[Rh(5-Me-Sal-IProp)(CO)$_2$] (0.040 g, 0.07 mmol) was dissolved in 2 ml acetone to which PPh$_3$ (0.022 g, 0.08 mmol) was added. The solvent was allowed to evaporate slowly resulting in a yellow product (yield: 0.031 g, 70%). IR (ATR): ν_{CO} 1955 cm^{-1}; UV/Vis (nm, mol^{-1} cm^{-1}): λ_{max} = 390 nm, ε = 3082; $^{31}P\{^1H\}$(161.0 MHz, DMSO) δ = 41.5 (d, $^1J_{Rh\text{-}P}$ = 159 Hz) ppm. ^{1}H NMR (400 MHz, Acetone) δ 8.48 (s,1H), 7.74(m, 6H), 7.43(m, 9H), 7.19(s, 1H), 6.34 (s, 1H), 6.07 (s, 1H), 3.96 (s, 1H), 2.30 (s, 3H), 1.92-1.24 (m 10H).

4.4. In situ characterization of Rh(III)-alkyl products [Rh([Rh(N,O-ScBa)(CO)(me)(I)(PPh$_3$)] (4a-4f)

The Rh(III)-alkyl products for all the Schiff base-tertiary phosphine ligands could not be isolated as clean products and were consequently only characterized *in situ*. Typical *in situ* characterization was by ^{31}P NMR and infrared spectroscopy in dichloromethane, with solutions as follows: to (6.0-10.0)$\times 10^{-3}$ M dichloromethane solutions of **1a**-**d**, **2a** and **3a**, ([Rh([Rh(*N,O*-ScBa)(CO)(PPh$_3$)]) were added iodomethane to yield [MeI] of 1×10^{-2} to 5×10^{-1} M, and the reactions were monitored for 12-24 h using time resolved IR and/or ^{31}P NMR spectroscopy. All reactions indicated only the formation of the alkyl products.

4a: IR (DCM): ν_{CO} 2054 cm^{-1}; $^{31}P\{^1H\}$ (161.0 MHz, DCM) δ = 20.3 (d, $^1J_{Rh\text{-}P}$ = 110 Hz) ppm.

4b: IR (DCM): ν_{CO} 2056 cm^{-1}; $^{31}P\{^{1}H\}$(161.0 MHz, DCM) δ = 22.3 (d, $^{1}J_{Rh\text{-}P}$ = 112 Hz) ppm.
4c: IR (DCM): ν_{CO} 2040 cm^{-1}; $^{31}P\{^{1}H\}$(161.0 MHz, DCM) δ = 21.3 (d, $^{1}J_{Rh\text{-}P}$ = 113 Hz) ppm.
4d: IR (DCM): ν_{CO} 2036 cm^{-1}; $^{31}P\{^{1}H\}$(161.0 MHz, DCM) δ = 19.7 (d, $^{1}J_{Rh\text{-}P}$ = 112 Hz) ppm.
4e: IR (DCM): ν_{CO} 2054 cm^{-1}; $^{31}P\{^{1}H\}$(161.0 MHz, DCM) δ = 20.6 (d, $^{1}J_{Rh\text{-}P}$ = 110 Hz) ppm.
4f: IR (DCM): ν_{CO} 2054 cm^{-1}; $^{31}P\{^{1}H\}$(161.0 MHz, DCM) δ = 20.3 (d, $^{1}J_{Rh\text{-}P}$ = 111 Hz) ppm.

4.5. X-ray structure determinations

The reflection data were collected at 100(2) K on a Bruker X8 ApexII 4 K diffractometer using MoKα radiation (λ = 0.71073 Å). The cell parameters were refined by SAINT-Plus [52] while SADABS [53] was used for absorption corrections. The structures were solved by direct methods and refined on F^2 using anisotropic displacement parameters for all non-hydrogen atoms. SHELXL-97 [54,55] and WinGX [56] were used for structure solutions and refinements, respectively. The molecular graphics were prepared with DIAMOND [57]. All aromatic hydrogens and methyl hydrogens were placed in geometrically idealized positions (C-H = 0.93 Å and 0.96 Å) and constrained to ride on their parent atoms with U_{iso}(H) = 1.2 U_{eq}(C) and U_{iso}(H) = 1.5 U_{eq}(C), respectively. The N-bound hydrogen atom was located from the electron density map and refined without any constraints.

4.6. Kinetic measurements

All kinetic measurements were carried out in atmospheric conditions. The UV/visible spectra were performed on a Varian Cary 50 Conc spectrophotometer with thermostated automated multicell changers, equipped with a Julabo F1-mV temperature cell regulator and accurate within 0.1 °C in 1.000(1) cm quartz tandem cuvette cells. The infrared data for the rhodium(I) complexes were recorded as liquid samples in dry dichloromethane in a NaCl cell on a Bruker Tensor 27 spectrometer from 2350-1600 cm^{-1}, equipped with a temperature cell regulator accurate within ±0.3 °C. Iodomethane is highly volatile and the solutions were prepared in a fume hood and the solution used immediately after preparation.

Acknowledgements

Financial assistance from the University of the Free State and the SA NRF is gratefully acknowledged. Opinions, findings, conclusions, or recommendations expressed in this material are those of the authors and do not necessarily reflect the views of the SA NRF. Drs. D.V. Kama and O.T. Alexander are acknowledged for the single crystal data collections and assistance with solving the structures.

Disclosure statement

The authors declare no conflict of interest.

Funding

We also express our gratitude towards SASOL, Dr. Gerdus Kemp and PETLabs Pharmaceuticals, the South African National Research Foundation (SA-NRF/THRIP), in particular funding under the Swiss-South Africa joint research programme (SSAJRP) from the SA NRF (UID: 107802) and the Swiss National Science Foundation (Project IZLSZ2_170856) and and the University of the Free State for financial support of this project.

ORCID

Pennie P. Mokolokolo http://orcid.org/0000-0002-8736-0177
Alice Brink http://orcid.org/0000-0002-2612-359X
Andreas Roodt http://orcid.org/0000-0002-7349-6436
Marietjie Schutte-Smith http://orcid.org/0000-0001-8935-7601

References

[1] H. Schiff. *Ann. Chem. Pharm.*, **131**, 118 (1864).
[2] H. Schiff. *Ann. Chem. Pharm.*, **140**, 92 (1866).
[3] W. Qin, S. Long, M. Panunzio, S. Biondi. *Molecules*, **18**, 12264 (2013).
[4] (a) A. Frei, P.P. Mokolokolo, R. Bolliger, H. Braband, M.S. Tsosane, A. Brink, A. Roodt, R. Alberto. *Chem. Eur. J.*, **24**, 10397 (2018). (b) A. Roodt, R.A. Alberto, A. Frei, P.P. Mokolokolo, R.K. Bolliger, A. Brink, D.V. Kama. PCT Patent Application No. PCT/IB2018/060506 VS Ref: P3490pc00-TM6JA/LD, WO2019/123409 A1 (27 June 2019).
[5] (a) A. Brink, R.E. Kroon, H.G. Visser, C.E.J. van Rensburg, A. Roodt. *New J. Chem.*, **42**, 5193 (2018). (b) A. Brink, H.G. Visser, A. Roodt. *Inorg. Chem.*, **52**, 8950 (2013). (c) A. Brink, H.G. Visser, A. Roodt. *J. Coord. Chem.*, **64**, 122 (2011).
[6] K. Lamb. In *Carbon Dioxide Utilization*, M. North, P. Styring (Eds.), Vol. **2**, pp. 21–38, De Gruyter, Oldenburg (2019).
[7] H. Dandachi, X. Hong, F. Ibrahim, H. Nasrallah, A. Zulauf, N. Jaber, M. Mellah, E. Schulz. *Vietnam J. Chem.*, **58**, 29 (2020).
[8] X. Chang, Q. Zhang, C. Guo. *Angew. Chem. Int. Ed. Engl.*, **59**, 12612 (2020). Published on Web. 14 February.
[9] S. Abubakar, M.D. Bala. *ACS Omega*, **5**, 2670 (2020)..
[10] M. Gopiraman, S. Saravanamoorthy, S. Ullah, A. Ilangovan, I.S. Kim, I.M. Chung. *RSC Adv.*, **10**, 2545 (2020).
[11] J.A. Labinger. *Organometallics*, **34**, 4784 (2015).
[12] L.M. Rendina, R.J. Puddephatt. *Chem. Rev.*, **97**, 1735 (1997).
[13] P.M. Maitlis, A. Haynes, G.J. Sunley, M.J. Howard. *J. Chem. Soc, Dalton Trans.*, 2187 (1996).
[14] A. Haynes, B.E. Mann, D.J. Gulliver, G.E. Morris, P.M. Maitlis, D.J. Gulliver, G.E. Morris. *J. Am. Chem. Soc.*, **113**, 8567 (1991).
[15] (a) P.W.N.M. van Leeuwen, *Homogeneous Catalysis: Understanding the Art*, Springer (2004). (b) G. Rothenberg, *Catalysis*, 1st Edn., Kluwer Academic Publishers, Dordrecht / Boston / London (2008).
[16] (a) S.S. Basson, J.G. Leipoldt, A. Roodt, J.A. Venter. *Inorg. Chim. Acta*, **128**, 31 (1987). (b) J. Conradie, G.J. Lamprecht, S. Otto, J.C. Swarts. *Inorg. Chim. Acta*, **328**, 191, (2002). (c) J.J.C. Erasmus, J.C. Swarts. *Polyhedron*, **17**, 2447 (1998). (d) J. Conradie, J.C. Swarts.

Organometallics, **28**, 1018 (2009). (e) M.M. Conradie, J. Conradie. *Inorg. Chim. Acta*, **361**, 208 (2008). (f) N.F. Stuurman, J. Conradie. *J. Organomet. Chem.*, **694**, 259 (2009).
[17] M.M. Conradie, P.H. van Rooyen, C. Pretorius, A. Roodt, J. Conradie. *J. Mol. Struct*, **1144**, 280 (2017).
[18] A. Brink, A. Roodt, G. Steyl, H.G. Visser. *Dalton Trans.*, **39**, 5572 (2010).
[19] J.J.C. Erasmus, J. Conradie. *Dalton Trans.*, **42**, 8655 (2013).
[20] J.G. Leipoldt, S.S. Basson, L.J. Botha. *Inorg. Chim. Acta*, **168**, 215 (1990).
[21] N.F. Stuurman, B.E. Buitendach, L. Twigge, P.J. Swarts, J. Conradie. *New J. Chem.*, **42**, 4121 (2018).
[22] G.J.J. Steyn, A. Roodt, J.G. Leipoldt. *Inorg. Chem.*, **31**, 3477 (1992).
[23] S. Warsink, P.D.K. Kotze, J.M. Janse Van Rensburg, J.A. Venter, S. Otto, E. Botha, A. Roodt. *Eur. J. Inorg. Chem.*, **2018**, 3615 (2018).
[24] S. Warsink, F.G. Fessha, W. Purcell, J.A. Venter. *J. Organomet. Chem.*, **726**, 14 (2013).
[25] A. Roodt, H.G. Visser, A. Brink. *Crystallogr. Rev.*, **17**, 241 (2011).
[26] K.G. van Aswegen, J.G. Leipoldt, I.M. Potgieter, G.J. Lamprecht, A. Roodt, G.J. van Zyl. *Transition Met. Chem.*, **16**, 369 (1991).
[27] C.-H. Cheng, B.D. Spivack, R. Eisenberg. *J. Am. Chem. Soc.*, **99**, 3003 (1977).
[28] (a) G.J.J. Steyn, A. Roodt, J.G. Leipoldt. *J. Am. Chem. Soc.*, **1**, 13597(2002). (b) L. Gonsalvi, H. Adams, G.J. Sunley, E. Ditzel, A. Haynes. *J. Am. Chem. Soc.*, **124**, 13597 (2002).
[29] (a) J.A. Venter, J.G. Leipoldt, R. van Eldik. *Inorg. Chem.*, **30**, 2207 (1991). (b) J.G. Leipoldt, S.S. Basson, L.J. Botha. *Inorg. Chim. Acta*, **168**, 215 (1990). (c) S. Warsink, A. Roodt, J.A. Venter, P.D.R. Kotze, S. Otto. Z. Kristallogr. *NCS*, **228**, 335 (2013). (d) S. Warsink, A. Roodt, J.A. Venter, P.D.R. Kotze, S. Otto. Z. Kristallogr. *NCS*, **228**, 428 (2013). (e) K.R. Koch. *Coord. Chem. Rev.*, **245**, 121 (2001).
[30] (a) L.O. Nindakova, N.M. Badyrova. *Mol. Catal.*, **486**, 110880 (2020). (b) A. Mannu, A. Grabulosa, S. Baldino. *Catalysts*, **10**, 162 (2020). (c) S. Shaw, J.D. White. *Chem. Rev.*, **119**, 9381 (2019). (d) K. Zhou, B. Chen, X. Zhou, S. Kang, Y. Xu, J. Wei. *Chem. Cat. Chem.*, **5562** (2019). (e) N.C.C. Breckwoldt, G.S. Smith, P. van der Gryp, N.J. Goosen. *J. Reac. Kinet. Mech. Cat.*, **128**, 333 (2019).
[31] A. Brink, H.G. Visser, A. Roodt. *J. Coord. Chem.*, **64**, 122 (2011).
[32] A. Brink, H.G. Visser, A. Roodt. *Polyhedron*, **52**, 416 (2013).
[33] A. Brink, A. Roodt, H.G. Visser. *Acta Crystallogr. Sect. E Struct. Rep. Online*, **65**, o3175 (2009).
[34] D.E. Graham, G.J. Lamprecht, I.M. Potgieter, A. Roodt, J.G. Leipoldt. *Transition Met. Chem.*, **16**, 193 (1991).
[35] G.J.J. Steyn, A. Roodt, J.G. Leipoldt. *Rhodium Express*, **1**, 25 (1993).
[36] G.J.J. Steyn, A. Roodt, I. Poletaeva, Y. Varshavsky. *J. Organomet. Chem.*, **536-537**, 197 (1997).
[37] G.J.J. Steyn, A. Roodt. *S. Afr. J. Chem.*, **2**, 242 (2001).
[38] A. Roodt, S. Otto, G. Steyl. *Coord. Chem. Rev.*, **245**, 125 (2003).
[39] K.A. Bunten, C. Moreno, A.J. Poë. *Dalton Trans.*, 1416 (2005).
[40] J.G. Leipoldt, S.S. Basson, J.T. Nel. *Inorg. Chim. Acta*, **74**, 85 (1983).
[41] J.G. Leipoldt, S.S. Basson, E.C. Grobler, A. Roodt. *Inorg. Chim. Acta*, **99**, 13 (1985).
[42] J.G. Leipoldt, S.S. Basson, C.R. Dennis. *Inorg. Chim. Acta*, **50**, 121 (1981).
[43] Y.S. Varshavsky, M.R. Galding, V.N. Khrustalev, I.S. Podkorytov, S.N. Smirnov, V.A. Gindin, A.B. Nikolskii. *J. Organomet. Chem.*, **761**, 123 (2014).
[44] J.M. Janse van Rensburg, A. Muller, A. Roodt. *Acta Crystallogr. E Struct. Rep. Online*, **63**, m3015 (2007).
[45] G. Steyl. *Polyhedron*, **26**, 5324 (2007).
[46] J.M. Janse van Rensburg, A. Roodt, A. Muller. *Acta Crystallogr. E Struct. Rep. Online*, **62**, m1040 (2006).
[47] (a) J.G. Leipoldt, R. van Eldik, S.S. Basson, A. Roodt. *Inorg. Chem.*, **25**, 4639 (1986). (b) A. Muller, S. Otto, A. Roodt. *Dalton Trans.*, **650** (2008). (c) S. Otto, O.T. Alexander, A. Roodt. *Suid-Afrikaanse Tydskrif vir Natuurwetenskap en Tegnologie/South African J. Sci. Technol.*,

38, 180 (2019). (d) A. Roodt, J.G. Leipoldt, L. Helm, A.E. Merbach. *Inorg. Chem.*, **33**, 140 (1994). (e) W. Purcell, A. Roodt, S.S. Basson, J.G. Leipoldt. *Transition Met. Chem.*, **14**, 224 (1989).

[48] M. Schutte-Smith, A. Roodt, H.G. Visser. *Dalton Trans.*, **48**, 9984 (2019).

[49] (a) G.J.J. Steyn, A. Roodt, J.G. Leipoldt. *Inorg. Chem.*, **31**, 3477 (1992). (b) G.J.J. Steyn, A. Roodt. *S. Afr. J. Chem.*, **54**, 9 (2001).

[50] (a) L.J. Damoense, W. Purcell, A. Roodt, J.G. Leipoldt. *Rhodium Express*, **5, 10** (1994). (b) L.J. Damoense. Ph.D. thesis, University of the Free State, Bloemfontein, South Africa (2001).

[51] G.J.S. Venter, G. Steyl, A. Roodt. *J. Coord. Chem.*, **67**, 176 (2014).

[52] *Bruker. SAINT-Plus.* Bruker AXA, Inc., Madison, Wisconsin, USA (2012).

[53] Bruker. *SADABS.* Bruker AXS, Inc., Madison, Wisconsin, USA (2012).

[54] G.M. Sheldrick. *Acta Crystallogr.*, **A64**, 11 (2008).

[55] G.M. Sheldrick, *SHELXL97*, University of Göttingen, Göttingen, Germany (1997).

[56] L.J. Farrugia. *J. Appl. Crystallogr.*, **32**, 837(1999).

[57] K. Brandenburg, H. Putz. *DIAMOND, release 3.1b*, *Crystal Impact GbR*, Bonn, Germany (2005).